Study on defect-free debinding green body of ceramic formed by DLP technology

Article (Accepted Version)

Study on defect-free debinding green body of ceramic formed by DLP technology

Kai Wang[a,1], Mingbo Qiu[a,1], Chen Jiao[a], Jiajun Gu[a], Deqiao Xie [a], Changjiang Wang[b], Xiaobing Tang[c], Zhen Wei[d], and Lida Shen[a,*]

[a] College of Mechanical and Electrical Engineering, Nanjing University of Aeronautics and Astronautics, Nanjing, 210016, China

[b] Department of Engineering and Design, University of Sussex, Sussex House, Brighton BN1 9RH, UK

[c] College of Materials Science and Technology, Nanjing University of Aeronautics and Astronautics, Yu Dao Street , 210016, Nanjing, China

[d] Jiangsu pharmaceutical association；Zhong Shan East Road, 210016, Nanjing, China

∗ Corresponding author.

∗∗ Corresponding author. College of Mechanical and Electrical Engineering, Nanjing University of Aeronautics and Astronautics, Nanjing, 210016, China.

E-mail addresses: ldshen@nuaa.edu.cn (L. Shen).

[1] These authors contributed equally

Abstract: Current research into the causes of macro-cracks in the debinding of light-cured ceramic body is predominantly focused on heating rate and holding time. In this paper, we propose a novel approach to analyze the causes of defects in the ceramic body during the debinding process via the interconnected channels formed in the process of the binder discharged from the inside to the outside. The physical and chemical changes, and related reaction products of the binder were analyzed by the

TG-FTIR using a specific resin as the binder in the low temperature debinding stage (200~300 ℃) and high temperature debinding stage（300~600 ℃）. Based on the result, a novel approach is proposed to illustrate the process of the formation of interconnected channels and defects. The samples of green bodies debond at different holding time were analyzed by the SEM and μ-CT. The experimental results prove the formation of interconnected channels, and it is found that the holding temperature of 237 ° C is favorable for the formation of the channel and the discharge of the gas products. The defect-free samples after low temperature debinding process were debond in the high temperature debinding process at three different holding temperatures of 360 °C, 430 °C, and 550 °C obtained by analyzing the DTG curve and the absorption curve of CO_2 in the infrared spectrum, and samples after high temperature debinding process were analyzed by the SEM and μ-CT. The experimental results show that these holding temperatures favor the stable discharge of CO_2 and the binder pyrolysis products from the channels, thereby avoiding cracks due to severe gas expansion. The research results in this paper have important reference value for the preparation of defect-free ceramic samples.

Keywords: Zirconia; digital light processing; thermal debinding; defects control

1. Introduction

The rapid development of additive manufacturing (3D printing) technology has stimulated the development of numerous ceramic additive manufacturing processes. Digital light processing (DLP) 3D-printing is one of the most commonly used

manufacturing methods [1-6]. It works by uniformly spreading ceramic powder in liquid photosensitive resin to prepare slurry. The crosslink reaction of liquid photosensitive resin in the UV exposure then causes the slurry to solidify, binding the ceramic powder together in a certain shape. The ceramic green body part is achieved by printing layer by layer. Through the subsequent thermal debinding process, the organic photosensitive resin component in the green body part is burned at high temperature to obtain the brown body part, which is then transformed into a densified ceramic part in the following sintering process. This process requires no mold design and material utilization is nearly 100%, reducing the manufacturing costs significantly.

Porous ceramic parts with complex structures can be manufactured efficiently using 3D printing [7-10]. During the debinding process, an excessive heating rate or inappropriate holding temperature or duration will often cause large cracks. In the subsequent sintering process, it is difficult to heal such cracks by the self-healing process of powder sintering, resulting in compromised mechanical strength of the sintered part [11, 12]. Chang Liu [13] studied stereolithography additive manufacturing technology for silica glass. Thermal gravimetric analysis (TGA) and Fourier transform infrared (FTIR) spectroscopy were utilized, illustrating that the debinding curve was optimized to effectively shorten the debinding time. Haidong Wu [14] used the stereolithography process to fabricate alumina ceramic parts and studied the effect of alumina powder particle size and the debinding process on the density of the final sintered parts. A sample containing nano-sized and micro-sized alumina particles was shown to possess higher density than the sample containing only nano-sized or

micro-sized alumina particles and the sample obtained via vacuum debinding had a higher density. Fatih [15] studied the shape retention properties of low-pressure injection molded (LPIM) zirconia during thermal debinding. The distinctive surface binder film was found to have healing and leveling effects on the surface defects, thus improving the strength of the parts. Emil [16] reduced the shrinkage of the organic binder during debinding by adding a non-reactive component to the photosensitive resin, further reducing delamination and intra-laminar cracks in the ceramic part. Maopeng Zhou [17] fabricated alumina cutting tool green body parts obtained by the stereolithography process and used a two-step debinding process (vacuum debinding followed by air atmosphere debinding) to control the pyrolysis rate of the binder to suppress the formation of defects. Pfaffinger [18] researched the thermal debinding of ceramic-filled photopolymers printed by DLP 3D-printing, finding that the shape and design of the printed part, as well as debinding and sintering strategies, significantly affect the mechanical strength of the final part.

In the process of preparing ceramics by stereolithography, the debinding step is highly important, and the quality of the debinding process will directly affect the final result of the sintering step that follows [19-22]. Factors affecting the quality of the debinding process include the binder [21], the type of debinding process [19], and the ceramic powder [20]. Most research on the thermal debinding of printed ceramic green body focuses on the temperature where the mass loss rate of the binder reaches extreme values. In this paper, porous zirconia ceramic green body is prepared by DLP technology using a special resin as binder. The quality changes of ceramic green body

and the physical and chemical changes of resin in the binder during the process of thermal debinding are analyzed by thermal gravimetry-Fourier transform infrared spectroscopy (TG-FTIR). Based on this analysis, the causes of defects in the process of thermal debinding are analyzed, and the results are used to prepare a defect-free porous zirconia thermal debinding ceramic sample. The findings in this paper provide important reference for the preparation of defect-free stereolithography ceramics.

2. Materials and Methods

2.1 Materials and components

The solid content of the WA004 type photosensitive resin-based zirconia slurry (Prismlab Technology, China) used in this paper is 40wt%, the particle size of zirconia is 270 nm (D50) and the chemical composition and crystalline structure of the zirconia is 5.35wt% Y_2O_3-dopoed zirconia (TZP). The SEM image of zirconia powder is shown in Fig.1 (A), zirconia particles exhibit an irregular shape with slight agglomeration. The relation between the solid loading, viscosity and shear rate of zirconia slurry is shown in Fig.1 (B), it can be concluded that the viscosity decreases with the increase of the shear rate and the viscosity decreases slowly, and there is no obvious shear-thinning phenomenon, which indicates that the slurry exhibited a relatively stable state under the action of shearing force, and the viscosity of the slurry does not change significantly. At the same time, this also indicates that the zirconia powder is uniformly distributed in the binder, and the slight agglomeration of the nanoparticles does not have a significant effect on the stability of the slurry. The photosensitive resin is a compound prepared

with bisphenol A epoxy acrylate (BAEA) as the photosensitive prepolymer, 1,6-hexanediol diacrylate (HDDA), neopentyl glycol diacrylate (NPGDA), methyl propane triacrylate (TMPTA) as the diluent monomer, and 2-hydroxy-2-methyl propiophenone (1173) and diphenyl (2,4,6-trimethyl benzoyl) phosphine oxide (TPO) as photo initiators. Moreover, the photosensitive prepolymer and diluent monomer individually account for approximately 50% of the total mass of photosensitive resin, and the quality of the photoinitiator is negligible.

2.2 DLP 3D-printing and green body

A custom-made 3D-printer with a DLP light source was used in this study. A schematic diagram of the preparation process of DLP ceramic green body is provided in Scheme 1, and a picture of the real product is shown in Fig. 2. In this process, the light source projects the shape of the part slice on the slurry liquid surface, and the exposed slurry is cross-linked into a solid state that binds the ceramic powder together, while the unexposed slurry remains liquid. After exposure, the platform is lowered by one layer thickness, and a doctor blade is used to apply the fresh slurry uniformly on the previously formed layer. The next layer becomes irradiated and reciprocated to obtain a 3D ceramic green body part.

The printed sample was an 18 mm×18 mm×3 mm porous mesh structure block with an array of 2 mm×2 mm holes. The model and the green body are illustrated in Fig. 2(A) and Fig. 2(B). After sample preparation, the green body was washed repeatedly with anhydrous alcohol, then dried before being utilized in the debinding process.

2.3 Measurements and characterizations

The debinding process was performed using a hot air circulation debinding furnace (Gaoge Instruments, China). The composition of the debinding process products were then analyzed using a thermagravimetric anaylzer (209F3 Thermogravimetric analyzer, Netzsch, Germany) and Fourier transform infrared spectroscopy (TENSOR27, Bruker, Germany) under the air flow (30 ml/min). The sample mass was 4 mg, and the test temperature rose from 30 ℃ to 700 ℃ at 10 ℃ per minute. The morphology of the samples before and after debinding and the distribution of the binder on the surface of the sample debond at various temperatures was characterized by scanning electron microscopy (S4800, Hitachi, Japan, SEM). The rheological curve of the slurry was characterized by the microscopic infrared rheometer (MAS60, Thermo fisher, American). A micro-computed tomography scanner (μ-CT) (FF35 CT; YXLON International, Germany) with a 17 μm resolution was then used to scan the samples after thermal debinding at 200 kV and 50 μA. The samples were rotated 360° in 0.36° steps during the acquisition.

3. Results and Discussion

3.1 Thermal gravimetric analysis

The TG/DSC（thermal gravimetric/ differential scanning calorimetry）results for the ceramic green body are shown in Fig. 3. From the TG/DSC curve, it can be observed that the mass loss of green body begins to occur when the temperature is between 200 ℃ and 300 ℃, with mass loss at approximately 1%. Between 300 ℃ and 600 ℃, the quality

decreases to 74% of the original quality. When the temperature is higher than 600 ℃, the quality of the parts do not change and the debinding process ends. Based on this, it is determined that the debinding process of ceramic green body can be divided into two stages: low temperature debinding (200~300 ℃) and high temperature debinding (300~600 ℃). From the DSC curve, it can be concluded that the thermal debinding reaction is an endothermic process when the temperature is lower than 320 °C, and with the increase of temperature and the debinding process, the debinding reaction releases a lot of heat until the end of the debinding process. In the following section, the physical and chemical changes of the binder are analyzed by combining the products of the debinding process.

3.2 Infrared spectrum analysis of debinding products

The infrared spectra of the products in the debinding process of ceramic green body at 150~300 ℃ are shown in Fig. 4 (A). The absorption peaks at 3731 cm^{-1} and 2360 cm^{-1} are respectively attributed to H_2O and CO_2. The double absorption peaks at 3590 cm^{-1} and 3560 cm^{-1} are attributed to the stretching vibration of O-H bond, and the double absorption peaks at 2954 cm^{-1} and 2867 cm^{-1} are attributed to the stretching vibration of C-H bond [23]. In addition, the absorption peak at 1742 cm^{-1} is attributed to the stretching vibration of carboxylic groups, which indicate that carboxylic acids exist in the products, and the absorption peak at 1646 cm^{-1} are due to the stretching vibration of C=C bond [20]. Additionally, the absorption at 1512 cm^{-1} and 1456 cm^{-1} is attributed to the stretching vibration of benzene ring skeleton, and the absorption peaks at 1294 cm^{-1}

and 1164 cm^{-1} are attributed to the stretching vibration of C-O-C and C=O bonds, respectively, indicating that esters exit in the heating products [24-27]. Finally, the absorption peak at 940 cm^{-1} is attributed to the stretching vibration of epoxy bonds [24]. The infrared spectra of the products from the debinding process of ceramic green bodies at 300~600 ℃ are shown in Fig. 4(B), and the types and distribution of functional groups are essentially the same as those illustrated.

In the process of light curing of DLP, under the action of ultraviolet rays, the C=C bonds of epoxy resin and diluent monomer are broken, and consecutive polymerization reaction occurs, crosslinking to form polymer [23]. In Fig. 4(A), the absorption peak of C = C bond gradually strengthens from 200 ℃, indicating that the polymer begins to decompose into photosensitive resins and diluent monomers. During the synthesis of bisphenol A epoxy acrylate, the epoxy group in epoxy resin is opened and esterified with acrylic acid, and the epoxy bond gradually disappears [25]. However, the absorption peak of epoxy group appears in the infrared spectra of products at 250 ℃ in Fig. 4(A) and (B), and gradually strengthens with the increase of temperature. This indicates that the photosensitive resin bisphenol A epoxy acrylate begins to decompose into epoxy resin and acrylic acid, and the epoxy group of epoxy resin is closed again, so the absorption peak of epoxy resin in infrared spectrum is gradually enhanced. At the same time, the increasing absorption peaks of C=C bonds in the infrared spectra at 200 ~ 300 ℃ also proves that the cured polymer has begun to decompose, and the decomposition product bisphenol A epoxy acrylate is also partially decomposed into epoxy resin and acrylic acid. According to the previous discussion, the enhanced

absorption peaks of C=O and C-O-C indicate the presence of esters in the heated products of green body, which may arise from gasified polymers and bisphenol A epoxy acrylate. The increasing absorption peaks of H_2O and CO_2 indicate that some of the heated products are burned in the air to produce H_2O and CO_2.

When the heating temperature is 300~600 ℃, the above-mentioned epoxy bonds, carboxyl groups, C-O-C, C=O, and C=C bonds still display strong absorption peaks in infrared spectra at 300~430 ℃. In addition, the absorption peaks of epoxy bonds C=O and C=C gradually weaken, and almost disappear in infrared spectra at 500 ℃. Meanwhile, as illustrated in Fig. 4(C), the absorption peak of CO_2 reaches a maximum at 430 ℃ and is still strong at 600 ℃. This indicates that the binder polymer in ceramic green body still melts and evaporates at 300~500 ℃, but this trend gradually weakens until it stops at 500 ℃. This trend can be supported by DSC curves in the Fig.3, when the temperature is 300 ~ 320 ℃, the debinding process is an endothermic reaction, which means that the binder still melts and evaporates. At the same time, a large amount of binder polymer and its decomposition products are decomposed and a high level of CO_2 is produced. The bonding agent polymer in ceramic green body gradually decreases, and this trend slowly diminishes until the debinding is complete. During this process, the quality of ceramic green body does not change. To summarize, in the heating range of 300~ 600 ℃, some of the binders still melt and evaporate, but the thermal decomposition of the binders and their decomposition products dominate.

The low boiling point product acrylic acid is produced by partial melting and decomposition of the binder at the low temperature debinding stage, and the melted

binder and gas products are discharged from the ceramic green body from inside to outside. At the high temperature debinding stage, the binder still melts partially, but with the increase of temperature, it decomposes and carbonizes rapidly, producing CO_2 and releasing a lot of heat under the action of oxygen.

3.3 Causes of debinding defects in ceramic green body

According to the results of infrared spectroscopy analysis, during the low temperature debinding stage (200~300 ℃), some binders melt and decompose (as shown in Scheme 2 (A)), the diluent monomers and acrylic acid produced by decomposition of the binder gasify at this time, and the melted binder has a certain fluidity. During the debinding process, the binder on the surface of the green body melts and evaporates first, and the decomposed gas spills over (as shown in the dotted frame in Scheme 2 (B)) and oxidized in the air. With the removal of binder on the surface of the green bodies, the gaseous binder and gaseous decomposition products in green bodies move from the inner part of the green body to the surface with the melted binder under the action of pressure after thermal expansion and capillary force between powders. Therefore, the fused binder evaporates further, and the gaseous decomposition products further spill over on the surface of the green body, thus realizing the removal of the binder (as shown in Scheme 2 (B). At the same time, with the discharge of melt binder and gaseous products, interconnected channels are formed along their internal and external transfer paths (as shown in Scheme2 (C)). Once the interconnected pores are formed in the green body, at the extreme heating rate, the volume of gaseous binder and gaseous

decomposition products increase sharply in the process of discharging, and the excessive pressure on the ceramic green body results in crack formation. However, this process is conducive to the rapid and stable removal of residual binders without cracking in the subsequent high temperature debinding process. In the high temperature debinding stage (300~600 ℃), the binder polymer and its decomposition products undergo intense pyrolysis at high temperature. Additionally, the residual carbon elements in the pyrolysis reaction are oxidized to produce CO_2 in the air. They release a large amount of heat, intensifying the carbonization reaction of the binder as well as the CO_2 and pyrolysis products from inside to outside (as shown in Scheme 2 (D)). The rapidly expanding CO_2 will not only aggravate the defects in the low temperature debinding stage, but also cause new cracks

In conclusion, in the low temperature debinding stage, the interconnected pore forms in the green body during the process in which the melted binder and the gaseous decomposition product discharge from inside to outside. This process eventually produces cracks under the influence of a dramatic increase of the volume of gaseous decomposition product. However, in the high temperature debinding stage, the binder decomposes and carbonizes at high temperature and the carbon element oxidizes rapidly in the air to release large amount of heat. This further accelerates the decomposition of the binders and the volume expansion of CO_2 to extrude the green body, resulting in cracks.

3.4 Defect control verification experiment

Based on the previous analysis, a method to control the defects in the debinding stage of ceramics is proposed. In the low temperature debinding stage of the ceramic green body, the melted binder and gaseous decomposition products are transferred from the inner part to the surface of the green body by holding at a specific temperature, then interconnected holes are formed in the green body. In the subsequent high temperature debinding stage, with the increase of temperature, these holes are beneficial for the rapid and steady discharge of the residual binder and produced CO_2 without cracks due to mass heat and gas expansion at the appropriate temperature.

To verify the proposed method, the following experiments were carried out. Samples were divided into three groups to maintain the same heating rate, and each group was heated to 120 ℃ and held for 2 hours. The purpose of this process was to remove the water. The samples were then heated to T_1 = 200 ℃, T_2 = 237 ℃, and T_3 = 250 ℃, respectively, maintained at the respective temperatures for 3 hours [14, 17-19], and then cooled to room temperature at the same cooling rate. The experimental debinding temperature curve is provided in Fig. 5(A) and a ceramic green body after debinding is shown in Fig. 6. With the increase of temperature, the surface of the debinding ceramic green body is brown, and the color gradually deepens, indicating that the binder has begun to carbonize in this heating range. With the increase of temperature, the degree of carbonization gradually deepens, and the removal of binders also increases. At the holding temperature of 250 ℃, there are obvious cracks in the debinding ceramic green body (as shown in Fig.6. (C)). The computed tomography (CT) scanning images in Fig. 6 (C1~C4) show that most of the cracks (indicated by the arrows) occur at the

right angle of the square hole where the stress is concentrated in the debinding process. It can be observed that with the increase of scanning depth, the length and scope of the cracks gradually decrease and the cracks slowly disappear. The crack diffusion from inside to outside also proves that interconnected internal channels are formed along this route, together with the discharge of melted binder and gas products. The gas volume expands rapidly and extrudes the internal passage, which is damaged and cracks are formed due to the excessive heat preservation temperature. The shrinkage and mass loss of samples at different holding temperatures is shown in Fig. 5 (B). With the increase of heat preservation temperature, the size shrinkage and mass loss of the sample increases with the rise of temperature. However, when the heat preservation temperature is 250 ℃, the speed of increase in length and width size, as well as mass loss, slows down. The shrinkage rate of length and width is 11.1%, and the mass loss is 14.32%. This illustrates that the diluent monomer part of the binder has been completely discharged at this holding temperature. At this time, the binder in the sample begins to partially carbonize, and the remaining binder rapidly decomposes and carbonizes at high temperature.

To study the change rule of the binder in the low temperature debinding stage, the surface morphologies and the distribution of pores (indicated by the arrows in Fig.7) on the surface of the ceramic body before debinding and the above three samples were observed by SEM, and the results are shown in Fig. 7. The surface morphology of the ceramic green body before debinding process is provided in Fig. 7(A), in which the white particles are zirconia ceramic powder particles. The binder was tightly wrapped

with zirconia ceramic powder, and the surface was complete and without pores. According to the morphology of the binder on the surface of the sample after debinding, it can be seen that the binder is still tightly encapsulated with ceramic particles when the holding temperature is 200 ℃ (as shown in Fig. 7(B)), but the thickness of the encapsulation decreases slightly compared with that before debinding. This indicates that the binder on the surface of the ceramic body had begun to melt, evaporate, and be removed. As the holding temperature rises to 237 ℃, the debinding sample surface is covered with film-like binder (as shown in Fig. 7(C)), and the sample surface binder increases compared with the previous samples (Fig. 7(B)). This process is due to the internal melted binder which is discharged from the inside to the outside under the action of gas pressure and capillary force, resulting in an increase of the binders on the surface of the green body. When the holding time is 250 ℃, only a few binders are present on the debinding sample surface, and ceramic particles begin to expose (as shown in Fig. 7(D)). At this time, most of the binder on the sample surface has been removed. From the surface morphology of the sample after debinding, with the increase of holding temperature, pores begin to appear on the surface of the sample after debinding, and the number of pores rises with the increase of temperature. When the holding temperature is 200 ℃, the binder on the surface of the sample begins to melt and evaporate, and a small part of the pore on the surface of the sample is produced (as shown in Fig. 7(B). When the holding temperature rises to 237 ℃, it can be observed from the label in Fig. 7(C) that a larger area of pores on the surface of the film-like binders begins to appear. This is due to the discharge of melted binder and gaseous

decomposition products from the inside out. When the holding temperature is 250 ℃, the pore distribution area on the sample surface is larger and the number of pores is increased (as shown in Fig. 7(D)). This is attributed to the excessive holding temperature, as well as the gas decomposition products spilling out sharply and a rapid expansion of gas volume which causes the cracks that are shown in Fig. 6(C). In summary, in the low temperature debinding stage, melted binder and gaseous decomposition products spill from the inside to the outside of the sample. This indicates that there are similar interconnected pores inside the sample. At the same time, it is found that a temperature of 237 ℃ is conducive to the smooth discharge of melted binders and gas products which form a stable internal channel. However, the pressure of gas expansion at this temperature is not enough to cause cracks, and a defect-free debinding sample is formed.

According to the previous analysis, in the high temperature debinding stage, the binder in the green body decomposes in large quantities, and the residual carbon elements are oxidized rapidly to form CO_2 and release heat. Accordingly, the proposed strategy to control defects in the high temperature debinding stage is detailed as follows: To ensure the formation of stable interconnected pores in the low temperature debinding stage, a holding temperature of 237 °C is required. Then, an appropriate temperature must be adopted to ensure that the CO_2 and a large amount of heat generated in the pyrolysis of binder are discharged smoothly along the channels formed during the low temperature debinding stage. According to the DTG curve in Fig. 3, the extremum points of mass loss rate appear at 360 °C, 430 °C, and 550 °C, respectively. Therefore,

360 °C, 430 °C, and 550 °C are directly set in the high temperature debinding stage for 2 hours. In the previous low temperature debinding process, interconnected holes are formed between the interior and the surface of the green body parts. Therefore, setting the holding temperature at the extreme point of mass loss rate could ensure that the green body could remove the binder composition quickly without cracking. The debinding temperature curve is provided in Fig. 8 (A). According to the curve, the obtained parts have no cracks, as illustrated in Fig. 8(B). And it can be concluded from the SEM image(Fig.8 (C)) of green body after debinding process that the binder in the green body has been completely removed, and the grain size on the surface of the green body is relatively uniform, and it is not affected by the agglomeration of the powder to form larger crystal grains. The CT scanning image (as shown in Fig. 8(B1~B3)) of the marked area in Fig. 8(B) demonstrate that no obvious microcracks are found on the scanning sections 0.5 mm, 1.5 mm, and 2.5 mm away from the surface of the green body. It can also be seen that in the high temperature debinding stage, the three holding temperatures of 360 °C, 430 °C, and 550 °C are helpful for the smooth discharge of CO_2 and heat though the interconnected pores formed in the low temperature debinding stage and to avoid the cracks caused by gas expansion.

4. Conclusions

In this paper, zirconia ceramic green body was prepared by DLP technology using a special formulation of photosensitive resin as binder, and our team has also used the same method to prepare ceramic green body of other materials (such as HA, AI_2O_3,

HA-ZrO_2) to obtain defect-free samples. Through analysis of TG-FTIR results and the surface morphology of the ceramic green body under different heating conditions, the causes of defect formation in the process of thermal debinding were determined as well as methods of defect control. The following conclusions were drawn:

(1)The thermal debinding process of ceramic body is divided into two stages: low temperature debinding stage and high temperature debinding stage. In the low temperature debinding stage, the binder is partly melted and gasified, and gaseous diluent monomer and acrylic acid are produced by decomposition. Under the action of heat and capillary force, the diluent monomer and acrylic acid are diffused from the surface of the body to form interconnected pores in the body. Excessive heating rate will accelerate the diffusion of gas products, resulting in cracks. In the high temperature debinding stage, the binder decomposes and carbonizes rapidly, and carbon elements generate CO_2 under the action of oxygen, releasing a large amount of heat. In this situation, CO_2 and heat is not smoothly discharged from the inside to the outside, resulting in cracks.

(2)After analyzing the causes of defect formation, a strategy to control defect formation is determined. The appropriate temperature must first be selected in the low temperature stage so that the melted binder and gaseous decomposition products can be discharged smoothly from the inside to the outside, and to form stable interconnected pores in the interior. The appropriate thermal insulation temperature is then selected in the high temperature debinding stage to ensure the thermal decomposition product CO_2 and heat of the binder discharge smoothly

from the channel formed in the low temperature debinding stage, so as to avoid severe gas expansion which creates cracks. At the same time, the heat preservation temperatures at low and high temperature debinding stages are 237 °C, 360 °C, 430 °C, and 550 °C, respectively. The heating curves of the entire debinding process were obtained in this study, and defect-free porous zirconia ceramic samples were successfully prepared.

Acknowledgements

This work is supported by National Key Laboratory of Science and Technology on Helicopter Transmission (Nanjing University of Aeronautics and Astronautics) (Grant No. HTL-A-19G011), National Natural Science Foundation of China (No.U1537105 and No.1532106), National Key Research and Development Plan (No. 2018YFB1105400) and Jiangsu Province Key Research and Development Program (No. BE2016010-3). The authors also extend their sincere thanks to those who contributed in instructions and experiments work.

References

[1] J. Deckers, J. Vleugels, J.P. Kruth, Additive manufacturing of ceramics: A review, J. Ceram. Sci. Technol. 5 (2014) 245–260. doi:10.4416/JCST2014-00032.

[2] L. Ferrage, G. Bertrand, P. Lenormand, D. Grossin, B. Ben-Nissan, A review of the additive manufacturing (3DP) of bioceramics: Alumina, zirconia (PSZ) and hydroxyapatite, J. Aust. Ceram. Soc. 53 (2017) 11–20. doi:10.1007/s41779-016-0003-9.

[3] R.B. Osman, A.J. van der Veen, D. Huiberts, D. Wismeijer, N. Alharbi, 3D-printing zirconia implants; a dream or a reality? An in-vitro study evaluating the dimensional accuracy, surface topography and mechanical properties of printed zirconia implant and discs, J. Mech. Behav. Biomed. Mater. 75 (2017) 521–528. doi:10.1016/j.jmbbm.2017.08.018.

[4] A. Zocca, P. Colombo, C.M. Gomes, J. Günster, Additive Manufacturing of Ceramics: Issues, Potentialities, and Opportunities, J. Am. Ceram. Soc. 98 (2015) 1983–2001. doi:10.1111/jace.13700.

[5] F.P.W. Melchels, J. Feijen, D.W. Grijpma, A review on stereolithography and its applications in biomedical engineering, Biomaterials. 31 (2010) 6121–6130. doi:10.1016/j.biomaterials.2010.04.050.

[6] M. Schwentenwein, P. Schneider, J. Homa, Lithography-Based Ceramic Manufacturing: A Novel Technique for Additive Manufacturing of High-Performance Ceramics, Adv. Sci. Technol. 88 (2014) 60–64. doi:10.4028/www.scientific.net/ast.88.60.

[7] W. Bian, D. Li, Q. Lian, W. Zhang, L. Zhu, X. Li, Z. Jin, Design and fabrication of a novel porous implant with pre-set channels based on ceramic stereolithography for vascular implantation, Biofabrication. 3 (2011) 0–7. doi:10.1088/1758-5082/3/3/034103.

[8] S. Kirihara, Additive manufacturing of ceramic components using laser scanning stereolithography, Weld. World. 60 (2016) 697–702. doi:10.1007/s40194-016-0331-y.

[9] H. Seitz, W. Rieder, S. Irsen, B. Leukers, C. Tille, Three-dimensional printing of

porous ceramic scaffolds for bone tissue engineering, J. Biomed. Mater. Res. - Part B Appl. Biomater. 74 (2005) 782–788. doi:10.1002/jbm.b.30291.

[10]R. He, W. Liu, Z. Wu, D. An, M. Huang, H. Wu, Q. Jiang, X. Ji, S. Wu, Z. Xie, Fabrication of complex-shaped zirconia ceramic parts via a DLP-stereolithography-based 3D printing method, Ceram. Int. 44 (2018) 3412–3416. doi:10.1016/j.ceramint.2017.11.135.

[11]I.A. Chou, H.M. Chan, M.P. Harmer, Effect of Annealing Environment on the Crack Healing and Mechanical Behavior of Silicon Carbide-Reinforced Alumina Nanocomposites, J. Am. Ceram. Soc. 81 (2005) 1203–1208. doi:10.1111/j.1151-2916.1998.tb02469.x.

[12]P. Greil, Generic principles of crack-healing ceramics, J. Adv. Ceram. 1 (2012) 249–267. doi:10.1007/s40145-012-0020-2.

[13]C. Liu, B. Qian, X. Liu, L. Tong, J. Qiu, Additive manufacturing of silica glass using laser stereolithography with a top-down approach and fast debinding, RSC Adv. 8 (2018) 16344–16348. doi:10.1039/c8ra02428f.

[14]H. Wu, Y. Cheng, W. Liu, R. He, M. Zhou, S. Wu, X. Song, Y. Chen, Effect of the particle size and the debinding process on the density of alumina ceramics fabricated by 3D printing based on stereolithography, Ceram. Int. 42 (2016) 17290–17294. doi:10.1016/j.ceramint.2016.08.024.

[15]F.A. Çetinel, W. Bauer, R. Knitter, J. Haußelt, Factors affecting strength and shape retention of zirconia micro bending bars during thermal debinding, Ceram. Int. 37 (2011) 2809–2820. doi:10.1016/j.ceramint.2011.04.076.

[16]E. Johansson, O. Lidström, J. Johansson, O. Lyckfeldt, E. Adolfsson, Influence of resin composition on the defect formation in alumina manufactured by stereolithography, Materials (Basel). 10 (2017). doi:10.3390/ma10020138.

[17]M. Zhou, W. Liu, H. Wu, X. Song, Y. Chen, L. Cheng, F. He, S. Chen, S. Wu, Preparation of a defect-free alumina cutting tool via additive manufacturing based on stereolithography – Optimization of the drying and debinding processes, Ceram. Int. 42 (2016) 11598–11602. doi:10.1016/j.ceramint.2016.04.050.

[18]M. Pfaffinger, G. Mitteramskogler, R. Gmeiner, J. Stampfl, Thermal Debinding of Ceramic-Filled Photopolymers, Mater. Sci. Forum. 825–826 (2015) 75–81. doi:10.4028/www.scientific.net/msf.825-826.75.

[19]Z. Wu, W. Liu, H. Wu, R. Huang, R. He, Q. Jiang, Y. Chen, X. Ji, Z. Tian, S. Wu, Research into the mechanical properties, sintering mechanism and microstructure evolution of Al2O3-ZrO2 composites fabricated by a stereolithography-based 3D printing method, Mater. Chem. Phys. 207 (2018) 1–10. doi:10.1016/j.matchemphys.2017.12.021.

[20]F. Yang, M.Z. Zhu, Fabrication of β-TCP Scaffold with Pre-Designed Internal Pore Architecture by Rapid Prototyping of Mask Projection Stereolithography, Mater. Sci. Forum. 921 (2018) 67–77. doi:10.4028/www.scientific.net/msf.921.67.

[21]A. Goswami, G. Srivastava, A.M. Umarji, G. Madras, Thermal degradation kinetics of poly(trimethylol propane triacrylate)/poly(hexane diol diacrylate) interpenetrating polymer network, Thermochim. Acta. 547 (2012) 53–61. doi:10.1016/j.tca.2012.08.006.

[22]D. An, H. Li, Z. Xie, T. Zhu, X. Luo, Z. Shen, J. Ma, Additive manufacturing and

characterization of complex Al2O3 parts based on a novel stereolithography method, Int. J. Appl. Ceram. Technol. 14 (2017) 836–844. doi:10.1111/ijac.12721.

[23]X. Zhang, Y. Xu, L. Li, B. Yan, J. Bao, A. Zhang, Acrylate-based photosensitive resin for stereolithographic three-dimensional printing, J. Appl. Polym. Sci. 136 (2019) 1–10. doi:10.1002/app.47487.

[23]Y. Wang, Z. Chen, F. Yu, Preparation of epoxy-acrylic latex based on bisphenol F epoxy resin, J. Macromol. Sci. Part A Pure Appl. Chem. 55 (2018) 205–212. doi:10.1080/10601325.2017.1410065.

[25]W. Zhang, B. Shentu, Z. Weng, Preparation and properties of heat and ultraviolet-induced bonding and debonding epoxy/epoxy acrylate adhesives, J. Appl. Polym. Sci. 135 (2018) 1–8. doi:10.1002/app.46435.

[26]J. Lin, Syntheses and Properties of Aromatic Polyamides and Polyimides Derived from, (1970).

[27]S.P. Rwei, J. Da Chen, Investigating the UV-curing performance for polyacrylated polymer in dendritic and regular conformation, Polym. Bull. 68 (2012) 493–505. doi:10.1007/s00289-011-0644-3.

Figure list:

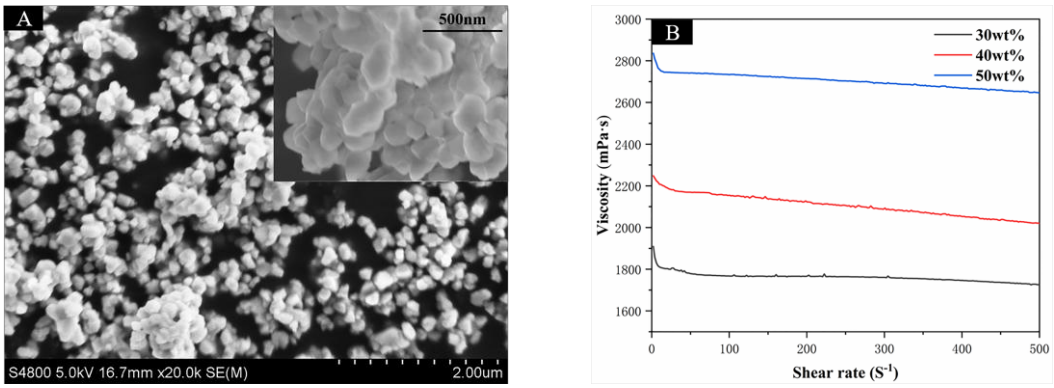

Fig. 1. SEM image of zirconia powder and rheological curve of the slurry：（A）The SEM image of zirconia powder;(B) The rheological curve of the slurry.

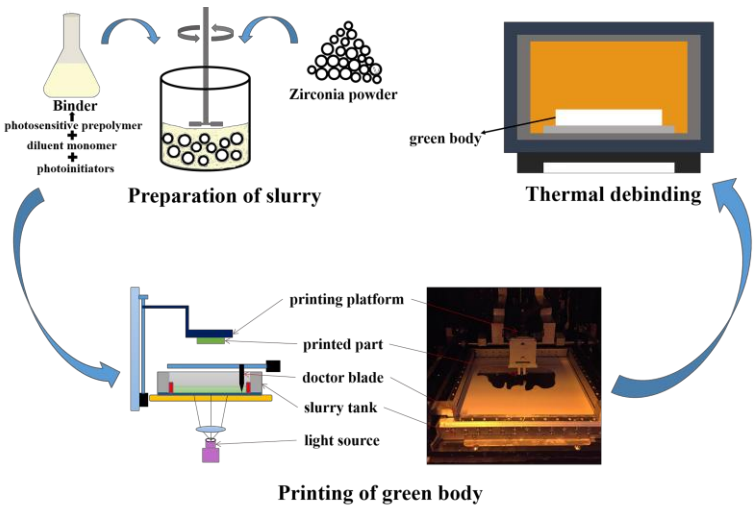

Scheme 1. Schematic illustration of the preparation process of DLP ceramic green body. The slurry is stirred with binder mixed with photosensitive prepolymer, diluent monomer, photoinitiators, and zirconia powder. The green body is prepared using a custom-made 3D printer with a DLP light source. The green body is utilized in the thermal debinding process, and the cause of defects in the green body during the debinding process is studied.

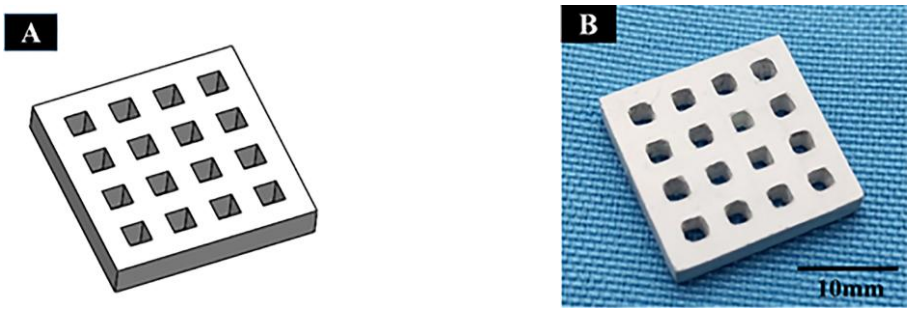

Fig. 2. Green body sample for debinding experiments: (A) 3D model of the sample; (B) Printed sample.

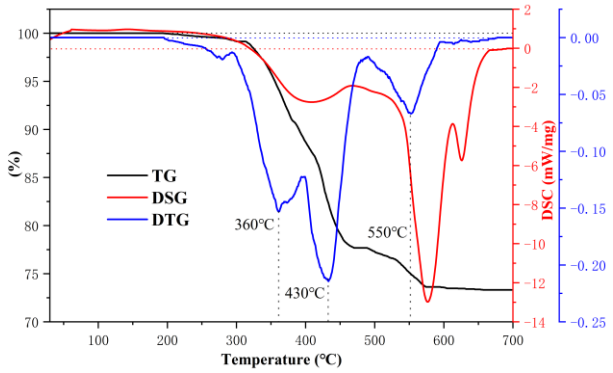

Fig. 3. TG/DSC curve of the printed zirconia ceramic green body sample.

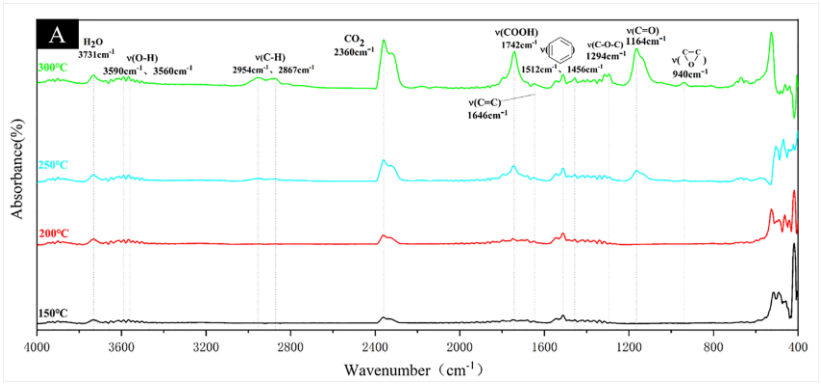

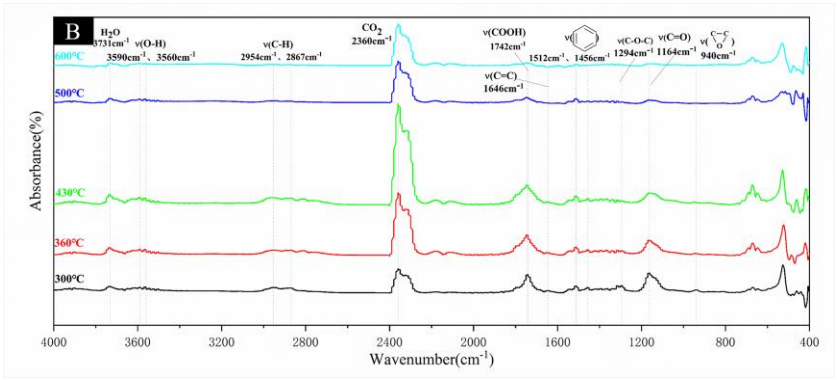

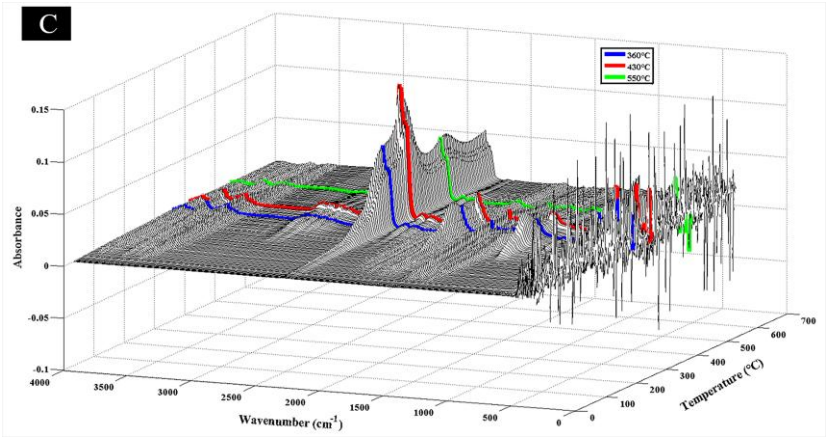

Fig. 4. Infrared absorption spectrogram of the ceramic green body:（A）Heated at 150~300 ℃;（B）heated at 300~600 ℃; (C) 3D infrared absorption spectrogram of the ceramic green body heated at 0~700 ℃.

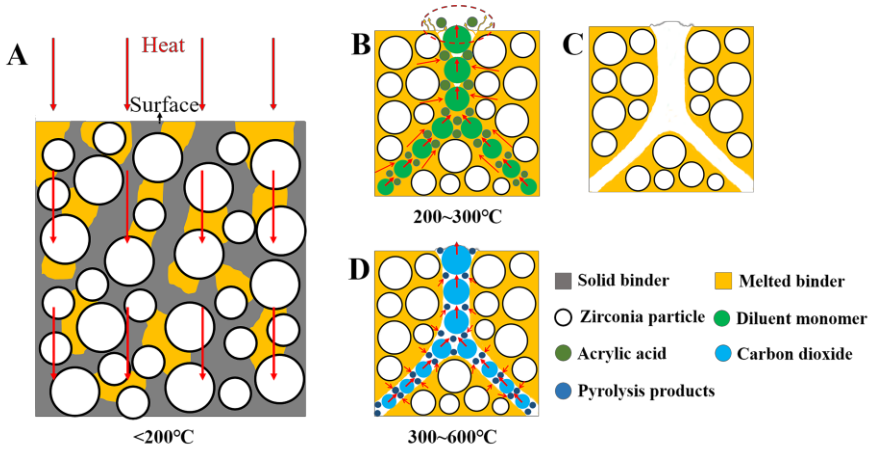

Scheme 2. Schematic diagram of the process of the binder discharging from the inner part of the green body to the surface:(A) The green body heated at 0~200 ℃, solid binder began to melt;(B) The green body heated at 200~300 ℃, gasified binder and acrylic acid gas moves from inside to outside of the green body in melted binder; (C) Schematic diagram of interconnected channels formed in the green body; (D) The green body heated at 300~600 ℃, pyrolysis products of binder and CO_2 gas discharge from inside to outside of the green body through interconnected channels.

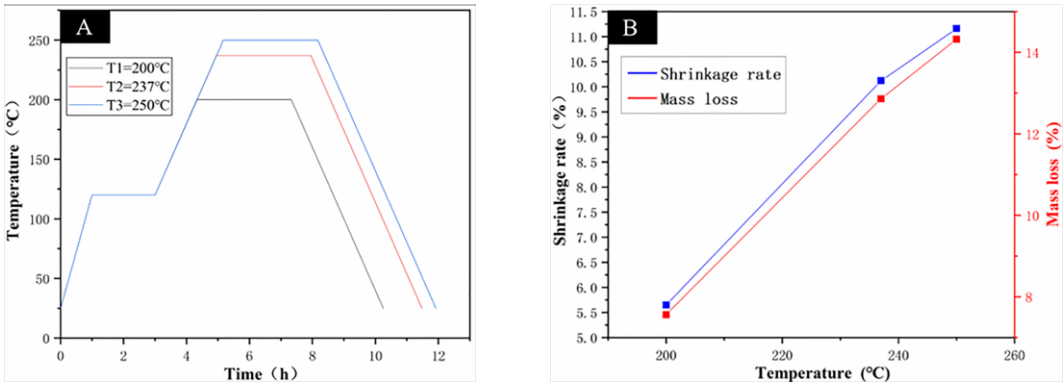

Fig. 5. Experimental debinding process and results of the sample: (A) Heating temperature curve of the sample; (B) Shrinkage rate and mass loss result of the sample.

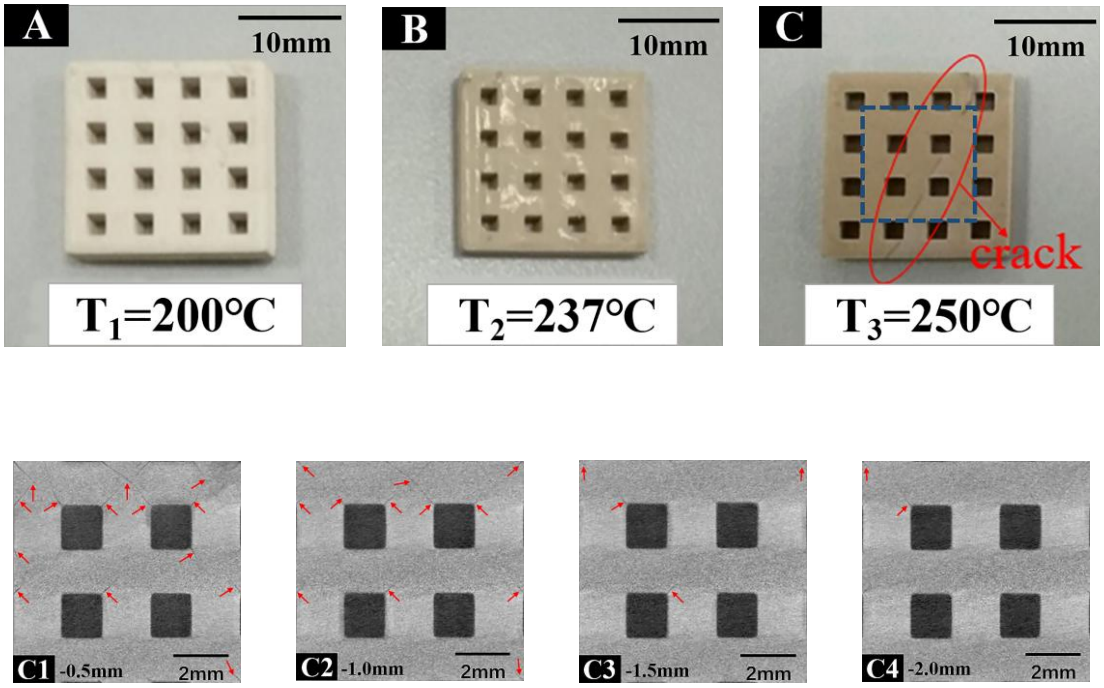

Fig. 6. Samples after heating at each temperature: (A) Heating at 200 ℃; (B) heating at 237 ℃; (C) heating at 250 ℃; (C1~C4) CT scanning images of different depths of surface area of green body marked by dotted frame in distance diagram (C) (-X mm represents the cross section of the green body from the surface of the green body).

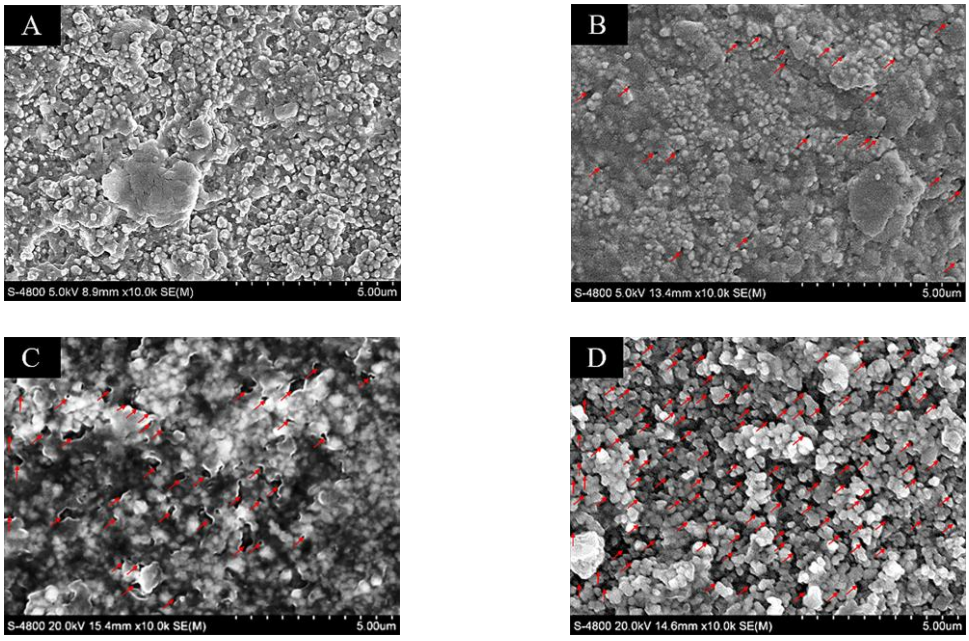

Fig. 7. SEM images of the surface of the samples after heating at each temperature: (A) Green body; (B) T_1=200 °C; (C) T_2=237 °C; (D) T_3=250 °C(The pores are indicated with red arrows).

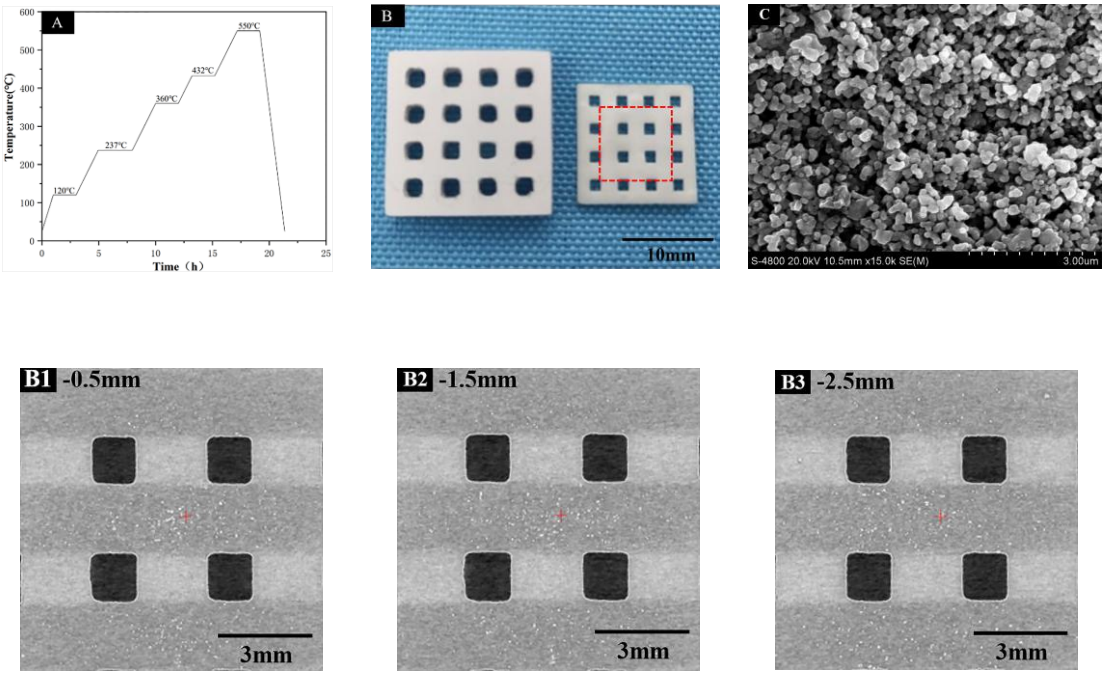

Fig. 8. Debinding curve and sintered defect-free sample: (A) Debinding curve of printed ceramic green body; (B) Printed sample (left) and sintered defect-free sample (right);

(B_1~B_3) CT scanning images of different depths of surface area of green body marked by dotted frame in distance (-X mm represents the cross section of the green body from the surface of the green body);(C) The SEM image of green body after debinding process.